1-1-1997

Study of Photon Dissociation in Diffractive Photoproduction at HERA

J. Breitweg
Argonne National Laboratory

M. Derrick
Argonne National Laboratory

D. Krakauer
Argonne National Laboratory

S. Magill
Argonne National Laboratory

D. Mikunas
Argonne National Laboratory

See next page for additional authors

Z. Phys. C 75, 421–435 (1997)

ZEITSCHRIFT
FÜR PHYSIK C

Study of photon dissociation in diffractive photoproduction at HERA

The ZEUS Collaboration

J. Breitweg, M. Derrick, D. Krakauer, S. Magill, D. Mikunas, B. Musgrave, J. Repond, R. Stanek, R.L. Talaga, R. Yoshida, H. Zhang
Argonne National Laboratory, Argonne, IL, USA[p]

M.C.K. Mattingly
Andrews University, Berrien Springs, MI, USA

F. Anselmo, P. Antonioli, G. Bari, M. Basile, L. Bellagamba, D. Boscherini, A. Bruni, G. Bruni, G. Cara Romeo, G. Castellini[1], L. Cifarelli[2], F. Cindolo, A. Contin, M. Corradi, S. De Pasquale, I. Gialas[3], P. Giusti, G. Iacobucci, G. Laurenti, G. Levi, A. Margotti, T. Massam, R. Nania, F. Palmonari, A. Pesci, A. Polini, G. Sartorelli, Y. Zamora Garcia[4], A. Zichichi
University and INFN Bologna, Bologna, Italy[f]

C. Amelung, A. Bornheim, I. Brock, K. Coböken, J. Crittenden, R. Deffner, M. Eckert, L. Feld[5], M. Grothe, H. Hartmann, K. Heinloth, L. Heinz, E. Hilger, H.-P. Jakob, U.F. Katz, E. Paul, M. Pfeiffer, Ch. Rembser, J. Stamm, R. Wedemeyer[6]
Physikalisches Institut der Universität Bonn, Bonn, Germany[c]

D.S. Bailey, S. Campbell-Robson, W.N. Cottingham, B. Foster, R. Hall-Wilton, M.E. Hayes, G.P. Heath, H.F. Heath, D. Piccioni, D.G. Roff, R.J. Tapper
H.H. Wills Physics Laboratory, University of Bristol, Bristol, U.K.[o]

M. Arneodo[7], R. Ayad, M. Capua, A. Garfagnini, L. Iannotti, M. Schioppa, G. Susinno
Calabria University, Physics Department and INFN, Cosenza, Italy[f]

J.Y. Kim, J.H. Lee, I.T. Lim, M.Y. Pac[8]
Chonnam National University, Kwangju, Korea[h]

A. Caldwell[9], N. Cartiglia, Z. Jing, W. Liu, J.A. Parsons, S. Ritz[10], S. Sampson, F. Sciulli, P.B. Straub, Q. Zhu
Columbia University, Nevis Labs., Irvington on Hudson, NY, USA[q]

P. Borzemski, J. Chwastowski, A. Eskreys, Z. Jakubowski, M.B. Przybycień, M. Zachara, L. Zawiejski
Institute of Nuclear Physics, Cracow, Poland[j]

L. Adamczyk, B. Bednarek, K. Jeleń, D. Kisielewska, T. Kowalski, M. Przybycień, E. Rulikowska-Zarębska, L. Suszycki, J. Zając
Faculty of Physics and Nuclear Techniques, Academy of Mining and Metallurgy, Cracow, Poland[j]

Z. Duliński, A. Kotański
Jagellonian Univ., Deptartment of Physics, Cracow, Poland[k]

G. Abbiendi[11], L.A.T. Bauerdick, U. Behrens, H. Beier, J.K. Bienlein, G. Cases[12], O. Deppe, K. Desler, G. Drews, U. Fricke, D.J. Gilkinson, C. Glasman, P. Göttlicher, J. Große-Knetter, T. Haas, W. Hain, D. Hasell, H. Heßling, K.F. Johnson[13], M. Kasemann, W. Koch, U. Kötz, H. Kowalski, J. Labs, L. Lindemann, B. Löhr, M. Löwe[14], J. Mainusch[15], O. Mańczak, J. Milewski, T. Monteiro[16], J.S.T. Ng[17], D. Notz, K. Ohrenberg[15], I.H. Park[18], A. Pellegrino, F. Pelucchi, K. Piotrzkowski, M. Roco[19], M. Rohde, J. Roldán, J.J. Ryan, A.A. Savin, U. Schneekloth, W. Schulz[20], F. Selonke, B. Surrow, E. Tassi, T. Voß[21], D. Westphal, G. Wolf, U. Wollmer[22], C. Youngman, A.F. Żarnecki, W. Zeuner
Deutsches Elektronen-Synchrotron DESY, Hamburg, Germany

B.D. Burow, H.J. Grabosch, A. Meyer, S. Schlenstedt
DESY-IfH Zeuthen, Zeuthen, Germany

G. Barbagli, E. Gallo, P. Pelfer
University and INFN, Florence, Italy[f]

G. Maccarrone, L. Votano
INFN, Laboratori Nazionali di Frascati, Frascati, Italy[f]

A. Bamberger, S. Eisenhardt, P. Markun, T. Trefzger[23], S. Wölfle
Fakultät für Physik der Universität Freiburg i.Br., Freiburg, Germany[c]

J.T. Bromley, N.H. Brook, P.J. Bussey, A.T. Doyle, D.H. Saxon, L.E. Sinclair, E. Strickland, M.L. Utley[24], R. Waugh, A.S. Wilson
Department of Physics and Astronomy, University of Glasgow, Glasgow, U.K.[o]

I. Bohnet, N. Gendner, U. Holm, A. Meyer-Larsen, H. Salehi, K. Wick
Hamburg University, I. Institute of Experimental Physics, Hamburg, Germany[c]

L.K. Gladilin[25], R. Klanner, E. Lohrmann, G. Poelz, W. Schott[26], F. Zetsche
Hamburg University, II. Institute of Experimental Physics, Hamburg, Germany[c]

T.C. Bacon, I. Butterworth, J.E. Cole, V.L. Harris, G. Howell, B.H.Y. Hung, L. Lamberti[27], K.R. Long, D.B. Miller, N. Pavel, A. Prinias[28], J.K. Sedgbeer, D. Sideris, A.F. Whitfield[29]
Imperial College London, High Energy Nuclear Physics Group, London, U.K.[o]

U. Mallik, S.M. Wang, J.T. Wu
University of Iowa, Physics and Astronomy Department, Iowa City, USA[p]

P. Cloth, D. Filges
Forschungszentrum Jülich, Institut für Kernphysik, Jülich, Germany

J.I. Fleck[30], T. Ishii, M. Kuze, M. Nakao, K. Tokushuku, S. Yamada, Y. Yamazaki[31]
Institute of Particle and Nuclear Studies, KEK, Tsukuba, Japan[g]

S.H. An, S.B. Lee, S.W. Nam, H.S. Park, S.K. Park
Korea University, Seoul, Korea[h]

F. Barreiro, J.P. Fernandez, R. Graciani, J.M. Hernández, L. Hervás, L. Labarga, M. Martinez, J. del Peso, J. Puga, J. Terron, J.F. de Trocóniz
Universidad Autónoma Madrid, Depto de Física Teóríca, Madrid, Spain[n]

F. Corriveau, D.S. Hanna, J. Hartmann, L.W. Hung, J.N. Lim, W.N. Murray, A. Ochs, M. Riveline, D.G. Stairs, M. St-Laurent, R. Ullmann
McGill University, Department of Physics, Montréal, Québec, Canada[a,b]

T. Tsurugai
Meiji Gakuin University, Faculty of General Education, Yokohama, Japan

V. Bashkirov, B.A. Dolgoshein, A. Stifutkin
Moscow Engineering Physics Institute, Mosocw, Russia[l]

G.L. Bashindzhagyan, P.F. Ermolov, Yu.A. Golubkov, L.A. Khein, N.A. Korotkova, I.A. Korzhavina, V.A. Kuzmin, O.Yu. Lukina, A.S. Proskuryakov, L.M. Shcheglova, A.V. Shumilin, A.N. Solomin, S.A. Zotkin
Moscow State University, Institute of Nuclear Physics, Moscow, Russia[m]

C. Bokel, M. Botje, N. Brümmer, F. Chlebana[19], J. Engelen, P. Kooijman, A. Kruse, A. van Sighem, H. Tiecke, W. Verkerke, J. Vossebeld, M. Vreeswijk, L. Wiggers, E. de Wolf
NIKHEF and University of Amsterdam, Amsterdam, Netherlands[i]

D. Acosta, B. Bylsma, L.S. Durkin, J. Gilmore, C.M. Ginsburg, C.L. Kim, T.Y. Ling, P. Nylander, T.A. Romanowski[32]
Ohio State University, Physics Department, Columbus, OH, USA[p]

H.E. Blaikley, R.J. Cashmore, A.M. Cooper-Sarkar, R.C.E. Devenish, J.K. Edmonds, N. Harnew, M. Lancaster[33], J.D. McFall, C. Nath, V.A. Noyes[28], A. Quadt, J.R. Tickner, H. Uijterwaal, R. Walczak, D.S. Waters, T. Yip
Department of Physics, University of Oxford, Oxford, U.K.[o]

A. Bertolin, R. Brugnera, R. Carlin, F. Dal Corso, U. Dosselli, S. Limentani, M. Morandin, M. Posocco, L. Stanco, R. Stroili, C. Voci
Dipartimento di Fisica dell' Universita and INFN, Padova, Italy[f]

J. Bulmahn, R.G. Feild[34], B.Y. Oh, J.R. Okrasiński, J.J. Whitmore
Pennsylvania State University, Department of Physics, University Park, PA, USA[q]

Y. Iga
Polytechnic University, Sagamihara, Japan[g]

G. D'Agostini, G. Marini, A. Nigro, M. Raso
Dipartimento di Fisica, Universita 'La Sapienza' and INFN, Rome, Italy[f]

J.C. Hart, N.A. McCubbin, T.P. Shah
Rutherford Appleton Laboratory, Chilton, Didcot, U.K.[o]

E. Barberis[33], T. Dubbs, C. Heusch, M. Van Hook, W. Lockman, J.T. Rahn, H.F.-W. Sadrozinski, A. Seiden, D.C. Williams
University of California, Santa Cruz, CA, USA[p]

O. Schwarzer, A.H. Walenta
Fachbereich Physik der Universität-Gesamthochschule Siegen, Siegen, Germany[c]

H. Abramowicz, G. Briskin, S. Dagan[35], T. Doeker, S. Kananov, A. Levy[36]
Raymond and Beverly Sackler Faculty of Exact Sciences, School of Physics, Tel-Aviv University, Tel-Aviv, Israel[e]

T. Abe, M. Inuzuka, K. Nagano, I. Suzuki, K. Umemori
Department of Physics, University of Tokyo, Tokyo, Japan[g]

R. Hamatsu, T. Hirose, K. Homma, S. Kitamura[37], T. Matsushita, K. Yamauchi
Tokyo Metropolitan University, Department of Physics, Tokyo, Japan[g]

R. Cirio, M. Costa, M.I. Ferrero, S. Maselli, V. Monaco, C. Peroni, M.C. Petrucci, R. Sacchi, A. Solano, A. Staiano
Universita di Torino, Dipartimento di Fisica Sperimentale and INFN, Torino, Italy[f]

M. Dardo
II Faculty of Sciences, Torino University and INFN - Alessandria, Torino, Italy[f]

D.C. Bailey, M. Brkic, C.-P. Fagerstroem, G.F. Hartner, K.K. Joo, G.M. Levman, J.F. Martin, R.S. Orr, S. Polenz, C.R. Sampson, D. Simmons, R.J. Teuscher[30]
University of Toronto, Department of Physics, Toronto, ON, Canada[a]

J.M. Butterworth, C.D. Catterall, T.W. Jones, P.B. Kaziewicz, J.B. Lane, R.L. Saunders, J. Shulman, M.R. Sutton
University College London, Physics and Astronomy Department, London, U.K.[o]

B. Lu, L.W. Mo
Virginia Polytechnic Institute and State University, Physics Department, Blacksburg, VA, USA[q]

J. Ciborowski, G. Grzelak[38], M. Kasprzak, K. Muchorowski[39], R.J. Nowak, J.M. Pawlak, R. Pawlak, T. Tymieniecka, A.K. Wróblewski, J.A. Zakrzewski
Warsaw University, Institute of Experimental Physics, Warsaw, Poland[j]

M. Adamus
Institute for Nuclear Studies, Warsaw, Poland[j]

C. Coldewey, Y. Eisenberg[35], D. Hochman, U. Karshon[35], D. Revel[35]
Weizmann Institute, Nuclear Physics Department, Rehovot 76100, Israel[d]

W.F. Badgett, D. Chapin, R. Cross, S. Dasu, C. Foudas, R.J. Loveless, S. Mattingly, D.D. Reeder, W.H. Smith, A. Vaiciulis, M. Wodarczyk
University of Wisconsin, Department of Physics, Madison, WI, USA[p]

S. Bhadra, W.R. Frisken, M. Khakzad, W.B. Schmidke
York University, Department of Physics, North York, ON, Canada[a]

[1] also at IROE Florence, Italy
[2] now at Univ. of Salerno and INFN Napoli, Italy
[3] now at Univ. of Crete, Greece
[4] supported by Worldlab, Lausanne, Switzerland
[5] now OPAL
[6] retired
[7] also at University of Torino and Alexander von Humboldt Fellow
[8] now at Dongshin University, Naju, Korea
[9] also at DESY and Alexander von Humboldt Fellow
[10] Alfred P. Sloan Foundation Fellow
[11] supported by an EC fellowship number ERBFMBICT 950172
[12] now at SAP A.G., Walldorf
[13] visitor from Florida State University
[14] now at ALCATEL Mobile Communication GmbH, Stuttgart
[15] now at DESY Computer Center
[16] supported by European Community Program PRAXIS XXI
[17] now at DESY-Group FDET
[18] visitor from Kyungpook National University, Taegu, Korea, partially supported by DESY
[19] now at Fermi National Accelerator Laboratory (FNAL), Batavia, IL, USA
[20] now at Siemens A.G., Munich
[21] now at NORCOM Infosystems, Hamburg
[22] now at Oxford University, supported by DAAD fellowship HSP II-AUFE III
[23] now at ATLAS Collaboration, Univ. of Munich
[24] now at Clinical Operational Research Unit, University College, London
[25] on leave from MSU, supported by the GIF, contract I-0444-176.07/95
[26] now a self-employed consultant
[27] supported by an EC fellowship
[28] PPARC Post-doctoral Fellow
[29] now at Conduit Communications Ltd., London, U.K.
[30] now at CERN
[31] supported by JSPS Postdoctoral Fellowships for Research Abroad
[32] now at Department of Energy, Washington
[33] now at Lawrence Berkeley Laboratory, Berkeley
[34] now at Yale University, New Haven, CT
[35] supported by a MINERVA Fellowship
[36] partially supported by DESY
[37] *present address:* Tokyo Metropolitan College of Allied Medical Sciences, Tokyo 116, Japan
[38] supported by the Polish State Committee for Scientific Research, grant No. 2P03B09308
[39] supported by the Polish State Committee for Scientific Research, grant No. 2P03B09208

Received: 21 April 1997

[a] supported by the Natural Sciences and Engineering Research Council of Canada (NSERC)
[b] supported by the FCAR of Québec, Canada
[c] supported by the German Federal Ministry for Education and Science, Research and Technology (BMBF), under contract numbers 057BN19P, 057FR19P, 057HH19P, 057HH29P, 057SI75I
[d] supported by the MINERVA Gesellschaft für Forschung GmbH, the German Israeli Foundation, and the U.S.-Israel Binational Science Foundation
[e] supported by the German Israeli Foundation, and by the Israel Science Foundation
[f] supported by the Italian National Institute for Nuclear Physics (INFN)
[g] supported by the Japanese Ministry of Education, Science and Culture (the Monbusho) and its grants for Scientific Research
[h] supported by the Korean Ministry of Education and Korea Science and Engineering Foundation
[i] supported by the Netherlands Foundation for Research on Matter (FOM)
[j] supported by the Polish State Committee for Scientific Research, grant No. 115/E-343/SPUB/P03/120/96
[k] supported by the Polish State Committee for Scientific Research (grant No. 2 P03B 083 08) and Foundation for Polish-German Collaboration
[l] partially supported by the German Federal Ministry for Education and Science, Research and Technology (BMBF)
[m] supported by the German Federal Ministry for Education and Science, Research and Technology (BMBF), and the Fund of Fundamental Research of Russian Ministry of Science and Education and by INTAS-Grant No.

Abstract. Diffractive dissociation of quasi-real photons at a photon-proton centre of mass energy of $W \approx 200$ GeV is studied with the ZEUS detector at HERA. The process under consideration is $\gamma p \to XN$, where X is the diffractively dissociated photon system of mass M_X and N is either a proton or a nucleonic system with mass $M_N < 2$ GeV. The cross section for this process in the interval $3 < M_X < 24$ GeV relative to the total photoproduction cross section was measured to be $\sigma_D^{partial}/\sigma_{tot} = 6.2 \pm 0.2(stat) \pm 1.4(syst)\%$. After extrapolating this result to the mass interval of $m_\phi^2 < M_X^2 < 0.05W^2$ and correcting it for proton dissociation, the fraction of the total cross section attributed to single diffractive photon dissociation, $\gamma p \to Xp$, is found to be $\sigma_{SD}/\sigma_{tot} = 13.3 \pm 0.5(stat) \pm 3.6(syst)\%$. The mass spectrum of the dissociated photon system in the interval $8 < M_X < 24$ GeV can be described by the triple pomeron ($I\!P I\!P I\!P$) diagram with an effective pomeron intercept of $\alpha_{I\!P}(0) = 1.12 \pm 0.04(stat) \pm 0.08(syst)$. The cross section for photon dissociation in the range $3 < M_X < 8$ GeV is significantly higher than that expected from the triple pomeron amplitude describing the region $8 < M_X < 24$ GeV. Assuming that this discrepancy is due to a pomeron-pomeron-reggeon ($I\!P I\!P I\!R$) term, its contribution to the diffractive cross section in the interval $3 < M_X < 24$ GeV is estimated to be $f_{I\!P I\!P I\!R} = 26 \pm 3(stat) \pm 12(syst)\%$.

1 Introduction

Interactions of real photons with protons at high energy bear many similarities to hadronic interactions. This can be understood in the framework of the vector meson dominance model (VDM) [1, 2], in which the photon is assumed to fluctuate into a virtual vector meson (ρ, ω, ϕ) prior to the interaction with the proton. The resulting collisions are expected to exhibit all the characteristics of a hadron-hadron reaction, including diffraction. Diffractive processes at high energies are generally characterized by an exponential suppression of the squared four momentum (t) transferred between the colliding particles and a weak energy dependence of the cross section. The colliding hadrons may emerge intact from the interaction (elastic scattering). Alternatively, one or both may be excited into more massive states – single or double diffractive dissociation, respectively. In all cases the hadronic final state is characterized by the presence of two groups of particles separated in rapidity.

The elastic and total cross sections for hadron-hadron collisions at high centre of mass (c.m.) energies have been successfully described in the Regge picture in terms of the exchange of two dominant trajectories: the pomeron and the reggeon [3]. The data from fixed target photoproduction experiments [2] combined with the recent measurements from HERA [4–7] also confirm the validity of this model for the description of the total photoproduction cross section as well as for the cross sections for the light vector meson production.

Regge theory in conjunction with Mueller's theorem [8] allows the modelling of single dissociation processes [9]. The measurements of pp and $p\bar{p}$ reactions up to the very high c.m. energies of $W = 1800$ GeV [10] show that the diffractive cross sections are dominated by the triple pomeron amplitude. The values of the pomeron intercept extracted from the shape of the dissociated mass spectra are consistent with those obtained from the total and elastic cross sections [11]. The diffractive dissociation of real photons has been previously studied at fixed target experiments reaching a c.m. energy of $W \approx 14$ GeV [12], where it was observed that the general properties of diffractive photoproduction are similar to those of hadronic reactions. It is thus of interest to test whether this similarity holds at higher energies.

In this paper we study the dependence of the cross section on the mass, M_X, of the dissociated photon system X for the diffractive process $\gamma p \to Xp$. The measurement was performed with the ZEUS detector at the HERA collider using ep collisions in which the virtuality Q^2 of the exchanged photon is smaller than $0.02\,\mathrm{GeV}^2$ and $W \approx 200$ GeV. A similar analysis has been performed recently by the H1 collaboration [13].

The paper is organized as follows. After a brief review of the basic concepts of the triple Regge phenomenology (Sect. 2), we describe the experimental setup, the trigger and the event selection criteria (Sects. 3, 4 and 5). The Monte Carlo (MC) models used for the acceptance corrections are described in Sect. 6, while Sect. 7 contains the presentation of the method used to reconstruct M_X. In Sect. 8 we describe the measurement of the M_X spectrum in events corresponding to the processes $\gamma p \to XN$, where N is either a proton or a nucleonic system with mass $M_N < 2$ GeV. In order to suppress the contribution from nondiffractive photoproduction processes only the events with a gap in the rapidity distribution of final state hadrons (rapidity-gap events) were included. The subtraction of the remaining contamination from nondiffractive processes and the correction for detector effects were performed using a MC simulation technique. The analysis of the M_X spectrum in the framework of Regge theory is described in Sect. 9. To test the sensitivity of the results to the model assumptions made in this study an alternative analysis of the same data sample was performed. No rapidity-gap was required and the distinction between the different processes was performed solely on the basis of the shape of the M_X spectrum. This alternative analysis is described in Sect. 10, which also contains a comparison between the results of the two methods. The paper concludes, in Sect. 11, with a comparison of the results with other experiments and with the expectations from Regge phenomenology.

2 Triple Regge model

The Regge model describes particle interactions in terms of the exchange of trajectories. Three trajectories are of primary importance, namely the pomeron, $\alpha_{I\!P}(t) = 1.08 + 0.25 \cdot t$,

93-63
[n] supported by the Spanish Ministry of Education and Science through funds provided by CICYT
[o] supported by the Particle Physics and Astronomy Research Council
[p] supported by the US Department of Energy
[q] supported by the US National Science Foundation

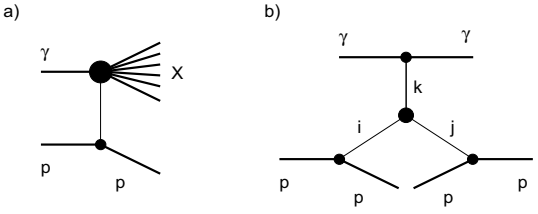

Fig. 1. The photoproduction processes related by Mueller's theorem: **a** the inclusive reaction $\gamma p \to Xp$ and **b** the triple Regge diagram of the three body scattering $\gamma pp \to \gamma pp$

the reggeon, $\alpha_{I\!R}(t) = 0.45 + t$ and the pion $\alpha_\pi(t) = 0 + t$. The trajectory parameters are not given by the model but are determined from data [11, 3]. Mueller's theorem [8] relates the inclusive cross section for the photoproduction reaction $\gamma p \to Xp$ (Fig. 1a) to the forward amplitude of the three body hadronic process $\gamma pp \to \gamma pp$. If M_X^2, W^2/M_X^2 and $W^2/|t|$ are large, the triple Regge diagram shown in Fig. 1b is expected to dominate the three body amplitude [14]. The triple Regge diagram predicts the following behaviour of the cross section [14]:

$$\frac{d^2\sigma}{dtdM_X^2} = \left(\frac{1}{W^2}\right)^2 \cdot \sum_{ijk} G_{ijk}(t) \times \left(\frac{W^2}{M_X^2}\right)^{\alpha_i(t)+\alpha_j(t)} M_X^{2\,\alpha_k(0)}, \quad (1)$$

where the indices i, j, k denote the Regge trajectories. The effective coupling strength, $G_{ijk}(t)$, is not predicted by the model and must be determined from the experimental data. In the process depicted in Fig. 1b only the trajectories denoted by i and j are exchanged between the colliding particles and they carry the four momentum squared t. The k trajectory is related, via the optical theorem, to the probability that either i or j couple to the photon [15].

Diffractive processes are attributed to the exchange of the pomeron. In the triple Regge regime two diagrams are of primary importance: $ijk = I\!P I\!P I\!P$ and $I\!P I\!P I\!R$ [11]. The former triple pomeron term leads to an inclusive cross section falling with M_X^2 approximately as $d\sigma/dM_X^2 \propto 1/M_X^2$. The $I\!P I\!P I\!R$ contribution is important only at lower diffractive masses as it gives a steeper M_X^2 dependence of the form $d\sigma/dM_X^2 \propto (1/M_X^2)^{1.5}$.

A number of other triple Regge terms have been found to give a contribution to the inclusive cross sections in hadron-hadron reactions [11], namely: $ijk = I\!R I\!R I\!P$ describing the reggeon exchange and $ijk = \pi\pi I\!P$ and $\pi\pi I\!R$ describing the exchange of a pion trajectory. However these terms give contributions which are negligible at low M_X and become comparable to diffractive pomeron exchange only at $M_X^2 \approx 0.05W^2$ [10, 11].

In this paper only the processes due to pomeron exchange are referred to as diffractive and are treated as signal. The processes due to reggeon and pion exchange are called non-diffractive and are considered backgrounds.

3 Experimental setup

The analysis is based on data collected in 1994 with the ZEUS detector. HERA operated at a positron energy of 27.5 GeV and a proton energy of 820 GeV, with 153 colliding bunches. In addition 15 positron and 17 proton bunches were left unpaired for background studies.

A detailed description of the ZEUS detector may be found elsewhere [16, 17]. Here, a brief description of the detector components most relevant for this analysis is given. Throughout this paper the standard ZEUS coordinate system is used, which has its origin at the nominal interaction point. The Z-axis points in the direction of the proton beam, called the forward direction, and the X-axis points towards the centre of the HERA ring.

For the energy measurement the high resolution depleted-uranium scintillator calorimeter (CAL) is used [18]. It is divided into three parts, forward (FCAL) covering the pseudorapidity[1] region $4.3 > \eta > 1.1$, barrel (BCAL) covering the central region $1.1 > \eta > -0.75$ and rear (RCAL) covering the backward region $-0.75 > \eta > -3.8$. Holes of $20 \times 20\,\mathrm{cm}^2$ in the centre of FCAL and RCAL accommodate the HERA beam pipe. Each of the calorimeter parts is subdivided into towers which in turn are segmented longitudinally into electromagnetic (EMC) and hadronic (HAC) sections. These sections are further subdivided into cells, which are read out by two photomultiplier tubes. Under test beam conditions, the energy resolution of the calorimeter was measured to be $\sigma_E/E = 0.18/\sqrt{E(\,\mathrm{GeV})}$ for electrons and $\sigma_E/E = 0.35/\sqrt{E(\,\mathrm{GeV})}$ for hadrons. The calorimeter noise, dominated by the uranium radioactivity, is in the range $15 - 19\,\mathrm{MeV}$ for EMC cells and $24 - 30\,\mathrm{MeV}$ for HAC cells.

The proton remnant tagger (PRT) is used to tag events with a rapidity-gap. It consists of two layers of scintillation counters installed perpendicular to the beam at $Z = 5.15$ m. The two layers are separated by a 2 mm thick lead absorber. Each layer is split into two halves along the Y-axis and each half is independently read out by a photomultiplier tube. The counters have an active area of dimensions $30 \times 26\,\mathrm{cm}^2$ with a hole of $6.0 \times 4.5\,\mathrm{cm}^2$ at the centre to accommodate the HERA beam pipe. The pseudorapidity range covered by the PRT is $4.3 < \eta < 5.8$.

The luminosity monitor [19] (LUMI) measures the rate of the Bethe-Heitler process $ep \to e\gamma p$. The detector consists of two lead-scintillator sandwich calorimeters, installed in the HERA tunnel. The one at $Z = -35$ m is designed to detect positrons scattered at very small angles and the one at $Z = -107$ m measures the photons emitted along the positron beam direction. In this analysis, signals in the LUMI positron calorimeter were used to tag photoproduction events with positrons scattered at angles up to about 5 mrad with respect to the positrons beam direction. The LUMI positron calorimeter was also used to measure the energy of the scattered positron, E'_e, and derive the energy of the exchanged quasi-real photon, E_γ, through the relation $E_\gamma = E_e - E'_e = 27.5\,\mathrm{GeV} - E'_e$.

The leading proton spectrometer (LPS) [20] detects charged particles scattered at small angles and carrying a substantial fraction of the incoming proton momentum. These particles remain in the beam pipe and their trajectory is measured by a system of position sensitive silicon

[1] Pseudorapidity η is evaluated from the relation $\eta = -ln(tan(\theta/2))$, where θ is a polar angle calculated with respect to the proton beam direction

micro-strip detectors installed very close to the proton beam at Z = 63.0 m, 81.2 m and 90.0 m. The track deflection induced by the magnets in the proton beam line is used for the momentum analysis of the scattered proton.

4 Trigger

ZEUS uses a three level trigger system. At the first level a coincidence between signals in the LUMI positron calorimeter and in the rear part of the uranium calorimeter was required. The small angular acceptance of the LUMI positron calorimeter implied that the virtuality of the exchanged photon was $Q^2 < 0.02\,\mathrm{GeV}^2$. The uranium calorimeter trigger required a measured energy deposit in the RCAL EMC section of more than 464 MeV (excluding the towers immediately adjacent to the beam pipe) or 1250 MeV (including those towers).

The second and the third trigger levels were mainly used to reject beam related background. Parts of the data stream were prescaled in order to reduce the high event rate resulting from the large photoproduction cross section.

5 Selection of photoproduction events

The sample of events satisfying the photoproduction trigger and used in this study consisted of 103k events from a luminosity of $0.7\,\mathrm{pb}^{-1}$. In the offline analysis the energy of the scattered positrons measured in the LUMI calorimeter was restricted to the range $12 < E'_e < 18$ GeV, thereby limiting the γp c.m. energy to the interval of $176 < W < 225$ GeV.

5.1 Calorimeter noise suppression and trigger correction

The offline data sample contained a small number of events accidentally accepted by the online trigger because of a photomultiplier discharge or calorimeter noise contributing to an energy sum sufficient to exceed the trigger threshold. Thus, in the offline analysis, each event was subject to a two step trigger correction procedure. In the first step a noise suppression algorithm was applied to the CAL data. All the EMC (HAC) cells with energy below 60 MeV (110 MeV) were excluded from the data. For isolated cells the thresholds were increased to 80 MeV (140 MeV). Isolated cells were also excluded if they corresponded to one of the known noisy readout channels or if the imbalance between the two corresponding PM tubes was too large, indicating a noise pulse. This noise suppression algorithm was developed using events collected with a random trigger. In the second step the corrected CAL energies were used to reevaluate the trigger decision. The photoproduction events that failed the offline reconstructed trigger were not used in the analysis.

5.2 Statistical background subtraction

The remaining contamination of the offline sample was of two types: the e-gas and the coincidence background. The contamination of the data sample from e-gas background was on average below 0.5%, and concentrated in the sample of events characterized by low energy deposits in CAL. It was statistically subtracted using events from beam crossings where the positron bunch was unpaired. Another type of background is due to events with accidental coincidence of the bremsstrahlung process ($ep \to e\gamma p$) triggering the LUMI positron calorimeter and some activity in the main detector satisfying the RCAL trigger. The contamination from this type of background is 2% on average. It was subtracted statistically exploiting the fact that a large fraction of these background events could be identified since the energy deposits in the LUMI positron and photon calorimeters summed up to the positron beam energy. The identified background events were included with negative weights into all of the distributions in order to compensate for the background events where the bremsstrahlung photon was not detected. A detailed description of the statistical background subtraction method may be found in [5, 21].

6 Monte Carlo simulation

6.1 Models

The diffractive photon dissociation process, $\gamma p \to Xp$, was simulated with a MC program based on the Nikolaev-Zakharov [22] (NZ) model interfaced to the Lund fragmentation scheme [23]. For the study of systematic uncertainties the same process was simulated with the EPSOFT [24] program developed in the framework of HERWIG 5.7 [25]. EPSOFT models the diffractive dissociation as a soft hadronic collision of the photon with the pomeron. The particle multiplicities and the momenta of the hadrons transverse to the photon-pomeron collision axis are simulated using parameterizations of existing diffractive data [26, 27], while the longitudinal momenta are generated uniformly in phase space. Initially, the cross sections assigned to the events generated by both of these MC programs were consistent with the triple pomeron relation assuming a pomeron intercept $\alpha_{I\!P}(0) = 1.08$. For the final analysis they were iteratively reweighted so as to give the best description of the measured distributions, notably the reconstructed mass spectrum (see Sect. 7).

Elastic production of vector mesons, $\gamma p \to Vp$ with $V \equiv \rho^\circ$, ω, ϕ, and the diffractive processes involving the dissociation of the proton, $\gamma p \to VN, XN$, were simulated using EPSOFT. In the latter case the cross section calculations relied on parameterizations of the $pp \to pp, pN$ data [9].

Soft, nondiffractive collisions of the proton with hadronic fluctuations of the photon were also generated using the EPSOFT program. The particle multiplicities and the transverse momenta of the hadrons were simulated using parameterizations of the hadron-hadron data [28] tuned to describe also the ZEUS data [27]. The longitudinal momenta were generated uniformly in phase space. The effect of leading baryon production was simulated in EPSOFT in accordance with results from $p\overline{p}$ data. In the limit where the momentum of the leading baryon is close to that of the initial proton, i.e. where the triple Regge approach applies, the EPSOFT simulation gives results consistent with the combination of

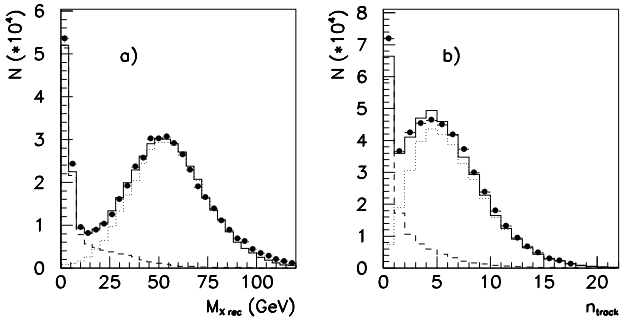

Fig. 2. The distribution of **a** the invariant mass of hadrons measured in the calorimeter (see Sect. 7) and **b** the multiplicity of charged tracks detected in the region of $-1.5 < \eta < 1.5$. The data are shown as *points* and the result of the MC simulation as a *solid line*. The diffractive and the nondiffractive components are also shown separately as *dashed* and *dotted histograms*, respectively

the reggeon and pion exchanges. The soft nondiffractive γp interactions from EPSOFT were enriched with hard, direct and resolved subprocesses simulated using HERWIG 5.7. The lower cut-off on the transverse momentum of the final-state partons, p_{Tmin}, was chosen to be 3 GeV. For the parton densities of the colliding particles, the GRV-LO [29] photon and MRSD$'_-$ [30] proton parameterizations were used. To cross check the sensitivity of the results to the nondiffractive model a sample of events generated with the multipartonic interaction option of PYTHIA 5.7 [31] was used.

All of the generated MC events were processed through the ZEUS detector simulation program based on GEANT and run through the same ZEUS reconstruction chain as the data. The events were then subject to the same CAL noise suppression algorithm and trigger requirements as the data.

6.2 Combination of the different MC samples

The different MC samples corresponding to the subprocesses discussed above were combined. In the first step the MC samples corresponding to the soft and hard nondiffractive components were combined with relative normalizations giving the best description of the measured transverse momentum distribution of charged tracks. In the next step the relative contribution of the diffractive and nondiffractive components was adjusted so as to reproduce the ratio between the number of events with no hits in the PRT and $8 < M_{X\,rec} < 20$ GeV (see Sects. 8.1 and 7) and the number of events with total CAL energy $E_{tot} > 60$ GeV in the data. The former data sample is dominated by diffractive processes with dissociated photon mass far from the region of low M_X resonances, while the latter consists mainly of nondiffractive events. In the MC simulation, the ratio of these two channels depends slightly on the characteristics of the simulated events. Therefore, this normalization procedure was performed independently for all the combinations of the MC models used. In all cases the results were consistent with the corresponding ratios between the measured photoproduction cross sections [4, 5]. The contribution from the vector meson production process was set to 15% of all the photon-proton interactions, as inferred from the HERA measurements [4–7].

The MC models used in this analysis were subject to a careful selection and tuning. The parameters defining the shapes of the hadronic final states were adjusted by comparing the distributions of multiplicity, polar angles and transverse momenta of charged tracks in the MC simulation to those measured [27]. As a result the Monte Carlo model correctly describes the general characteristics of photoproduction events at $W \approx 200$ GeV and there is good agreement between the data and the simulation for all relevant kinematical variables. An example is presented in Fig. 2 which shows a comparison between data and MC for the invariant mass of the hadronic system measured in the CAL (see below) and the multiplicity of charged tracks measured in the interval $-1.5 < \eta < 1.5$.

7 Mass reconstruction

In the kinematic region of diffractive photoproduction at HERA the dissociated photon system is produced nearly at rest in the laboratory system. Therefore, most of the particles from the photon dissociation are produced within the geometric acceptance of the CAL, and M_X may be approximated by the measured invariant mass of the hadronic system:

$$M_{X\,rec} = \sqrt{E^2 - P^2} \approx \sqrt{(E - P_Z) \cdot (E + P_Z)} = \sqrt{2E_\gamma \cdot (E + P_Z)}, \quad (2)$$

where E_γ is the energy of the exchanged photon and E is the energy of the hadronic system observed in the CAL. The total momentum of the hadronic system, P, approximately equals the longitudinal component, P_Z, as the transverse component is very small in the case of photoproduction events. The following formula was used for the mass reconstruction:

$$M_{X\,rec} \equiv a_1 \cdot \sqrt{2(E_e - E_{e'}) \cdot (\sum_{cond} E_i + \sum_{cond} E_i cos\theta_i)} + a_2. \quad (3)$$

The energy of the scattered positron, $E_{e'}$, was measured in the LUMI positron calorimeter. The quantities E_i and θ_i denote the energy and the polar angle of CAL condensates, defined as groups of adjacent cells with total energy of at least 100 MeV, if all the cells belong to the EMC, or 200 MeV otherwise.

In order to test the sensitivity of the M_X measurement to low energy particles which suffer from larger energy losses in the inactive material before entering the CAL, the whole analysis was repeated using only condensates of at least 200 MeV. The difference in the result is used for the estimate of the systematic error. The coefficients a_1 and a_2 correct for the effects of energy loss in the inactive material and energy deposits below the threshold. Their values, $a_1 = 1.14$ and $a_2 = 1.2$ GeV, were selected so as to give the best estimate of the true invariant mass in diffractive photon dissociation events from the MC simulation.

Figure 3 illustrates the quality of the diffractive mass reconstruction in the events from the MC simulation. The masses in the range $4 < M_X < 40$ GeV are reconstructed with an approximate resolution of $\sigma(M_X)/M_X \approx$

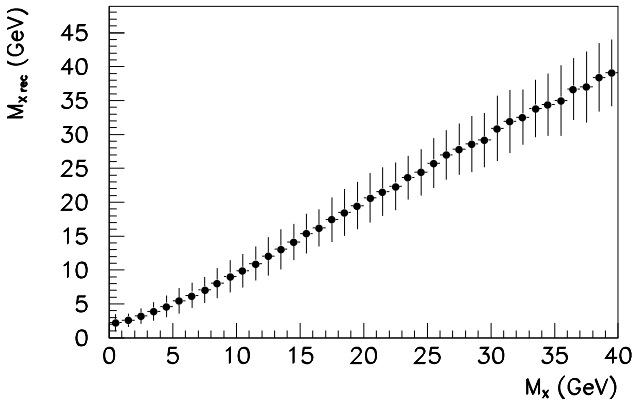

Fig. 3. The relation between the generated and the reconstructed mass of the dissociated photon in diffractive photoproduction events simulated using the EPSOFT MC program. The error bars show the r.m.s. of the reconstructed mass

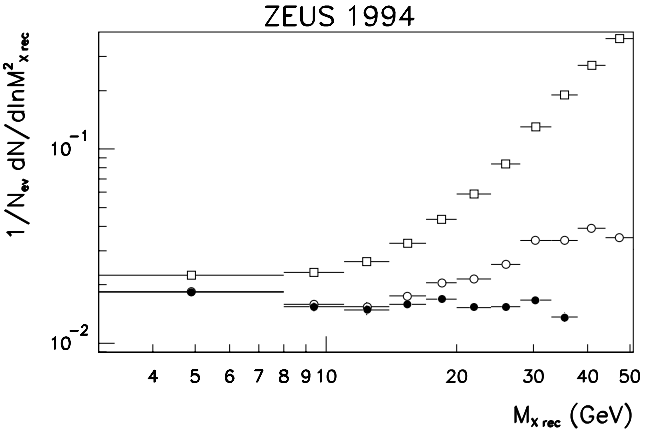

Fig. 4. Uncorrected spectrum of reconstructed hadronic mass in photoproduction events at $W \approx 200$ GeV before (*squares*) and after (*open circles*) imposing the requirement of no hits in the PRT. The latter spectrum was subject to subtraction of the nondiffractive contamination resulting in the uncorrected distribution attributed to diffractive processes (*solid points*)

$80\%/\sqrt{M_X}$ and an offset smaller than 0.5 GeV. The quality of the mass reconstruction has also been verified in the data using the events where the scattered proton was measured in the LPS. In these events the invariant mass of the hadronic system was estimated from the relation $M_X^2 \approx W^2 \cdot (1 - x_L)$, where $x_L = p'_p/p_p$ is the fraction of the initial momentum retained by the scattered proton. The distribution of the difference between the mass reconstructed from CAL and that estimated from the LPS shows a gaussian peak corresponding to contained events, i.e. where the entire X system was detected in CAL, and long tails due to events where some of the hadrons escaped detection through the beam pipe hole. For events with $4 < M_X < 45$ GeV the centre of the peak was at 0 ± 0.5 GeV confirming that the M_X reconstruction using the calorimeter showed no significant shifts.

At very low masses, $M_X < 2$ GeV, the mass reconstruction in CAL suffers from migrations towards higher values of $M_{X\,rec}$ due to the limited angular resolution of the calorimetric measurement. To reduce these migrations an additional cut was applied which accepted only events with at least one CAL deposit with energy $E > 400$ MeV at pseudorapidity $\eta_{max} > -1.5$.

8 Diffractive M_X spectrum in rapidity-gap events

The spectrum of the reconstructed hadronic mass is shown in Fig. 4 (open squares). It is presented in the form:

$$\frac{1}{N_{ev}} \cdot \frac{\Delta N}{\Delta \ln M^2_{X\,rec}}, \tag{4}$$

where ΔN denotes the number of events reconstructed in a given $\Delta \ln M^2_{X\,rec}$ interval and N_{ev} is the total number of events accepted by the trigger and passing the general selection criteria described in Sect. 5. The variable bin width, $\Delta \ln M^2_{X\,rec}$, was adjusted such as to keep the purity for diffractive events above 70%.

Diffractive processes are expected to give a contribution that is approximately flat in such a double logarithmic plot, and should dominate the region of low masses. The steep rise of the spectrum at higher values of $M^2_{X\,rec}$ is due to a large contribution from nondiffractive processes.

8.1 Selection of rapidity-gap events

In order to suppress the contamination from nondiffractive processes, only the events with a forward gap in the rapidity distribution of the final state hadrons were used. This rapidity-gap cut rejected all events with hits in the PRT detector. A hit was defined as a coincidence of signals of at least 50 ADC counts from both scintillator counter layers. The 50 counts threshold should be compared to the r.m.s. of the apparatus noise of 17 counts and to the $70 - 100$ counts corresponding to a minimum ionizing particle. The uncorrected $M_{X\,rec}$ distribution in events with no hits in the PRT is also shown in Fig. 4 as the open circles. The PRT cut softens the rise at high values of $M_{X\,rec}$ by reducing the contribution from nondiffractive processes. The remaining rise of the open circle points comes from nondiffractive processes which do not produce hits in the PRT counters. Before we correct for those, we first describe the response of the PRT detector to nondiffractive photoproduction processes.

8.2 PRT response to nondiffractive processes

The efficiency of the PRT counters to veto nondiffractive events was studied with the EPSOFT and PYTHIA MC generators. It was found that there are two factors which affect this efficiency. The first factor is related to the correlation between the multiplicity of particles produced in the PRT angular region ($4.3 < \eta < 5.8$) and the invariant mass of hadrons emitted in the angular region covered by the CAL. This multiplicity diminishes with decreasing mass of the hadronic system. Such behaviour is partially due to nondiffractive processes with pion and reggeon exchange that contribute mainly to the region of low $M_{X\,rec}$ and may produce events with rapidity-gaps. As a consequence, the fraction of nondiffractive events which have a particle (with energy above 1 GeV) emitted into the angular region of the PRT decreases from 99% at very high masses ($M_{X\,rec} \sim 70$ GeV), to about 85% at intermediate masses (~ 20 GeV) and to $\sim 75\%$ at lower masses (~ 12 GeV).

The second factor which affects the efficiency comes from the particle absorption in the material in front of the

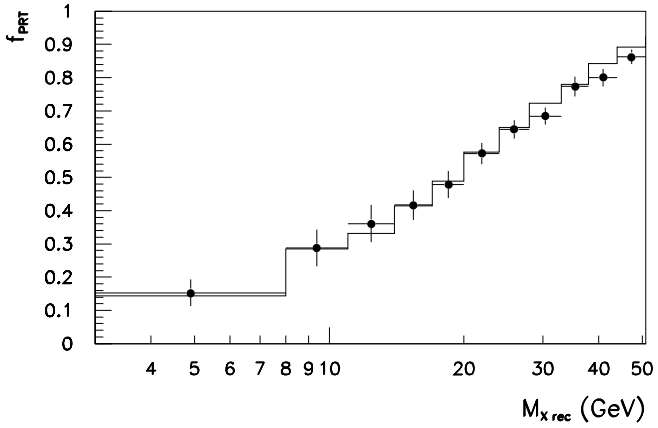

Fig. 5. The fraction of events with a PRT hit as function of the reconstructed mass $M_{X\,rec}$ for data (*solid points*) and for MC (*line*)

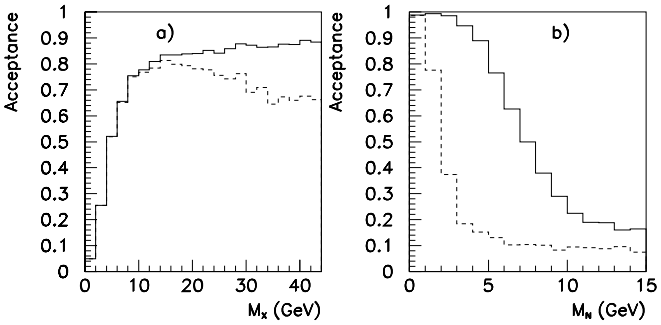

Fig. 6. a The combined acceptance of the trigger and the $\eta_{max} > -1.5$ cut for diffractive processes obtained from MC simulation (*solid line*). The effect of adding the requirement of no hits in PRT is also shown (*dashed line*). **b** The acceptance for proton dissociation, calculated as the fraction of events due to the process $\gamma p \to XN$ that are reconstructed with low mass in CAL, $M_{X\,rec} < 24$ GeV, (*solid line*) and have no hits in the PRT (*dashed line*)

PRT. Using a detailed modelling of the detector in the beam pipe region, the probability for a particle emitted inside the PRT acceptance to give a coincidence signal in the two layers of the detector was determined as a function of the particle production angle and energy. It was found that particles with $5.0 < \eta < 5.8$ have a probability of more than 99% to produce a coincidence signal in the PRT. Particles with $4.3 < \eta < 5.0$ have a high probability to be absorbed before reaching the PRT and on average only 30% of them will produce a coincidence signal.

The efficiency of the PRT to detect nondiffractive events depends on the two effects described above. In the MC simulation this efficiency varies from 95% at very high masses to about 75% at $M_{X\,rec} \sim 20$ GeV and 65% at $M_{X\,rec} \sim 12$ GeV. The reliability of the MC simulation was tested by comparing the fraction of events with the PRT tag as a function of the invariant mass observed in the CAL for the data and the MC simulation, including all the photoproduction subprocesses. This comparison is presented in Fig. 5 and shows good agreement between data and MC over the whole mass region used in this study.

The sensitivity of the results to the noise and the inefficiencies of the counters was investigated by repeating the whole analysis using slightly modified criteria for rejecting events with particle activity in the PRT: no coincidence between the two scintillator layers was required and the events with more than 50 counts signal in either of the counters were rejected. The difference between the results obtained using this and the original selection method was used for the estimate of the systematic uncertainty.

8.3 Subtraction of remaining nondiffractive contribution

The contribution of nondiffractive processes that survived the PRT rapidity-gap cut was estimated by using a MC simulation technique. By using the nondiffractive and the diffractive MC samples combined according to the procedure described in Sect. 6.2, the fraction of the cross section due to diffractive reactions was calculated for each $\ln M^2_{X\,rec}$ bin. This was then used to scale the measured spectrum, resulting in the distribution shown in Fig. 4 as solid points. This distribution needs to be corrected for acceptance, as discussed below. Note that the subtraction is reliable at low masses where the nondiffractive component is small. As the mass grows the nondiffractive contribution increases, reaching 40% of the signal at $M_{X\,rec} \approx 24$ GeV making the measurements beyond this point quite model dependent.

8.4 Acceptance for diffractive processes

The combined acceptance of the calorimeter trigger and the selection cuts for diffractive $\gamma p \to Xp$ events with $176 < W < 225$ GeV and $Q^2 < 0.02$ GeV^2 is presented in Fig. 6a as a function of M_X. At low masses, in particular in the region of light vector meson production, the acceptance is very low due to CAL trigger inefficiency and the $\eta_{max} > -1.5$ cut. For $M_X > 10$ GeV the acceptance rises to over 80%, where the trigger inefficiency is the main limiting factor. If the rapidity-gap cut based on the PRT is imposed, the acceptance for the diffractive photon dissociation in the mass region used for the measurement, $M_X < 24$ GeV, changes by less than 7%. For larger M_X the acceptance falls since the particles from the decay of the dissociated photon system reach the PRT.

In Fig. 6b the acceptance for the proton dissociation events $\gamma p \to XN$ with $M_X < 24$ GeV that appear in the sample of events with reconstructed mass $M_{X\,rec} < 24$ GeV is shown. With increasing M_N the acceptance diminishes, falling below 50% for $M_N > 7$ GeV, since the particles from the decay of the system N reach the CAL and thus $M_{X\,rec}$ is artificially large and beyond the region under study. If the PRT cut is used, the acceptance drops below 50% already at $M_N \approx 2$ GeV, resulting in a lower contribution of proton dissociation processes.

8.5 Acceptance correction

The uncorrected diffractive mass spectrum shown as solid points in Fig. 4 was corrected for detector effects by means of a multiplicative correction function, calculated using the MC:

$$Corr(M_X) = \left(\frac{1}{N_{gen}} \cdot \frac{\Delta N^{diff}_{gen}}{\Delta \ln M^2_{X\,gen}}\right) / \left(\frac{1}{N_{rec}} \cdot \frac{\Delta N^{diff}_{rec}}{\Delta \ln M^2_{X\,rec}}\right). \quad (5)$$

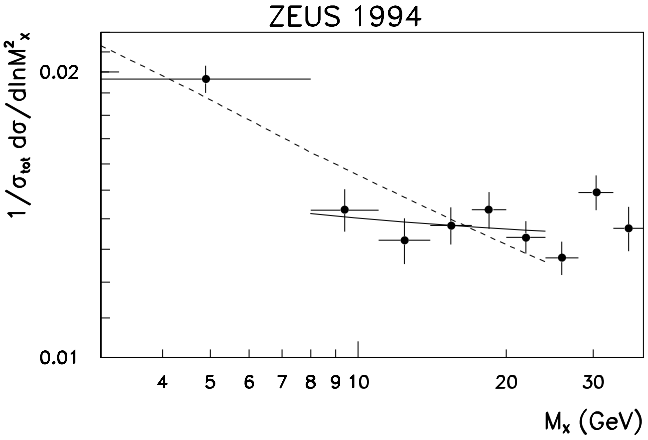

Fig. 7. The acceptance corrected M_X spectrum in diffractive photoproduction events. The combined statistical errors of the data and of the correction factors are shown as *vertical bars*. The line indicates the result of the fits of (6) to the diffractive spectrum in the intervals $3 < M_X < 24$ GeV (*dashed line*) and $8 < M_X < 24$ GeV (*solid line*)

Here ΔN_{rec}^{diff} denotes the number of diffractive MC events with no hits in the PRT that are reconstructed in the considered $\Delta \ln M_{X\,rec}^2$ interval and N_{rec} is the number of MC events (including nondiffractive processes) passing the trigger and the general selection criteria. The quantity N_{gen} denotes the total number of MC events used for the calculation (including nondiffractive processes), while ΔN_{gen}^{diff} is the number of diffractive MC events with $M_N < 2$ GeV that were generated in the interval $\Delta \ln M_{X\,gen}^2$. The value of the correction factor $Corr(M_X)$ is in the range $0.9 - 1.1$ apart from the first mass bin, $3 < M_{X\,rec} < 8$ GeV, where it is close to 1.6. This method corrects for the following effects:

- the limited trigger acceptance and the inefficiencies of the event selection cuts (see solid line in Fig. 6a);
- the reduction of the acceptance for diffractive processes in the region of high M_X values due to PRT cut (see dashed line in Fig. 6a);
- smearing of the limit on the nucleonic mass $M_N < 2$ GeV due to the PRT acceptance (see Fig. 6b);
- migration effects in the mass reconstruction procedure.

8.6 Corrected M_X spectrum in diffractive events

Figure 7 presents the corrected M_X spectrum in diffractive photoproduction events. The quantity plotted corresponds to the probability per unit $\ln M_X^2$ that a photoproduction event with $W \approx 200$ GeV is due to a diffractive process $\gamma p \to XN$, where N is either a proton or a nucleonic system with $M_N < 2$ GeV. Apart from the first bin, $3 < M_X < 8$ GeV, the distribution is flat in the double logarithmic plot as expected for the diffractive processes dominated by the triple pomeron amplitude.

9 Analysis of M_X spectrum in rapidity-gap events

9.1 Diffractive cross section

By summing over the contents of the bins of the mass spectrum of Fig. 7 the fraction of the total photoproduction cross section attributed to photon dissociation, $\gamma p \to XN$, with $3 < M_X < 24$ GeV and $M_N < 2$ GeV is determined to be $\sigma_D^{partial}/\sigma_{tot} = 6.2 \pm 0.2(stat)\%$.

9.2 Shape of the M_X spectrum

The diffractive mass spectrum obtained from the rapidity-gap data was fitted in the range $3 < M_X < 24$ GeV with (1) evaluated for the triple pomeron case, $ijk = I\!P I\!P I\!P$, and integrated over t up to the kinematic limit t_{max}:

$$\frac{d\sigma}{d\ln M_X^2} = M_X^2 \frac{d\sigma}{dM_X^2} = M_X^2 \int_{-\infty}^{t_{max}} \frac{d^2\sigma}{dt dM_X^2} dt \propto \frac{M_X^2}{b_\circ + 2\alpha'_{I\!P} \ln \frac{W^2}{M_X^2}} \cdot \left(\frac{1}{M_X^2}\right)^{\alpha_{I\!P}(0)}. \quad (6)$$

The parameter values of $\alpha'_{I\!P} = 0.25\ \mathrm{GeV}^{-2}$ [9] and $b_\circ = 4\ \mathrm{GeV}^{-2}$ [12] were assumed in accord with results of experiments at lower energies. For the fit the function was integrated over each of the bins and the obtained values were compared with the corresponding number of data events.

As the result of the fit a pomeron intercept of $\alpha_{I\!P}(0) = 1.20 \pm 0.02(stat)$ was obtained, although with a poor χ^2 (see dashed curve in Fig. 7). A similar fit performed only for the range $8 < M_X < 24$ GeV gives a lower value of $\alpha_{I\!P}(0) = 1.12 \pm 0.04(stat)$ and provides a good description of the data in the fitted mass interval (see solid curve in Fig. 7). As the values of the pomeron intercept obtained from the triple-pomeron fit show some dependence on the fitting interval, this parameter will be referred to as an effective intercept.

9.3 The $I\!P I\!P I\!R$ component

If the function fitted in the range $8 < M_X < 24$ GeV is extrapolated to the region of the first bin, it falls significantly below the data point. A possible explanation is the contribution of a $I\!P I\!P I\!R$ term in addition to the triple pomeron amplitude. The precision of the data is insufficient to perform a reliable fit to the sum of the two components and to determine their relative contributions, as well as the pomeron and the reggeon intercepts. We have nevertheless verified that the obtained spectrum is consistent with the intercepts $\alpha_{I\!P}(0) = 1.08$ and $\alpha_{I\!R}(0) = 0.45$ derived from fits to total and elastic cross sections. Assuming these values we performed a fit of the sum of the $I\!P I\!P I\!P$ and the $I\!P I\!P I\!R$ terms to the entire interval of $3 < M_X < 24$ GeV. The fit indicates that the $I\!P I\!P I\!R$ term amounts to $26 \pm 3(stat)\%$ of the diffractive cross section in the considered M_X range. As shown in Fig. 8 the function obtained (solid line) is in good agreement with the data. The dotted line shows the fraction of the cross section attributed to the triple pomeron term alone, with an assumed pomeron intercept of $\alpha_{I\!P}(0) = 1.08$.

9.4 Single diffractive cross section

As discussed earlier, we measured the relative cross section for the diffractive process $\gamma p \to XN$ with $3 < M_X$

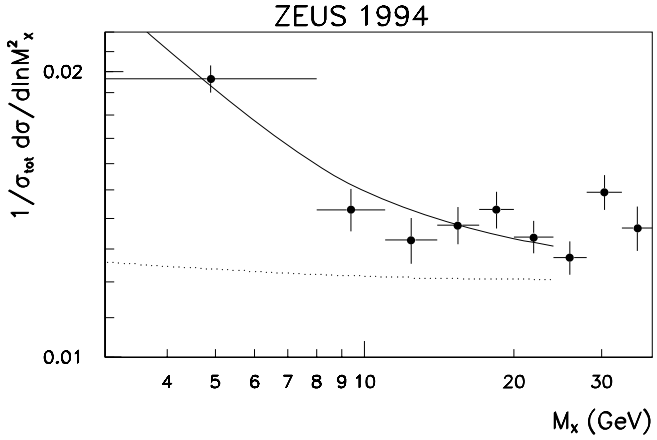

Fig. 8. The acceptance corrected M_X spectrum in diffractive photoproduction events fitted with the sum of a $I\!P I\!P I\!P$ and a $I\!P I\!P I\!R$ triple Regge terms (*solid line*). The contribution of the triple pomeron term is shown as a *dotted line*

< 24 GeV and $M_N < 2$ GeV as well as the shape of the M_X spectrum in this kinematic region. Using these data we estimated the fraction of the total photoproduction cross section that can be attributed to single diffractive photon dissociation. This was done by means of an analytic extrapolation of the M_X spectrum beyond the measured interval using the parameterization based on the sum of the $I\!P I\!P I\!P$ and the $I\!P I\!P I\!R$ terms. The parameterization was integrated from the ϕ meson mass, the heaviest of the three light vector mesons contributing to elastic photoproduction, up to $M_X^2 = 0.05 \cdot W^2$. The small contribution of proton excitation with $M_N < 2$ GeV was corrected for by assuming that the probability for the proton to be excited is the same as in pp reactions, namely $5 - 6\%$ [9]. The resulting ratio of the cross section for the single diffractive photon dissociation to the total photoproduction cross section is $\sigma_{SD}/\sigma_{tot} = 13.3 \pm 0.5(stat)\%$.

9.5 Systematic uncertainties

The systematic uncertainties in the results were studied by repeating the analysis using various event selection and acceptance correction methods and by changing the fit parameters within reasonable limits. The difference in the obtained results was used as an estimate of the uncertainty. Table 1 summarizes the outcome of the checks.

The largest uncertainty is due to the dependence of the result on the way the nondiffractive contribution is modelled. This effect was estimated by using PYTHIA to simulate the nondiffractive interactions instead of EPSOFT (see Sect. 6). Another important source of systematic error is related to the noise and the efficiency of the PRT. The corresponding uncertainty was evaluated by repeating the analysis without requiring the coincidence between the two layers of counters, as discussed in Sect. 5. The sensitivity to the model of diffractive processes used for the acceptance correction was checked by repeating the analysis using the EPSOFT generator instead of the NZ one (see Sect. 6).

In addition to these dominant sources of systematic error a number of other effects were studied. The cross section for vector meson production was changed by the size of the error, i.e. $\pm 3\%$, to check how the results depend on the simulated M_X behaviour in the region of low mass resonances (see Sect. 6). The sensitivity to the precision of the diffractive mass reconstruction was verified by using an alternative method of M_X determination that does not rely on low energy CAL condensates (see Sect. 7). To estimate the uncertainty due to imprecise calibration of the CAL trigger, the whole analysis was repeated with higher trigger thresholds. The energy thresholds applied to the data and to the MC were raised from 464 MeV(1250 MeV) to 660 MeV(1875 MeV) for the RCAL EMC trigger excluding (including) the towers adjacent to the beam pipe. To check the stability of the fitting procedure, the fit was repeated using mass intervals extended to $M_X = 32$ GeV. To examine the dependence of the result on the assumed parameter values, the t slope parameter was changed from $b_\circ = 4\,\mathrm{GeV}^{-2}$ to $5\,\mathrm{GeV}^{-2}$ and $\alpha'_{I\!P} = 0.20\,\mathrm{GeV}^{-2}$ was used instead of the original value of $0.25\,\mathrm{GeV}^{-2}$. To estimate the overall systematic uncertainty, all contributions were added in quadrature.

9.6 Results

We summarize here the results of the analysis based on the rapidity-gap data in photoproduction at $W \approx 200$ GeV:

- The fraction of the total photoproduction cross section attributed to the photon dissociation, $\gamma p \to XN$, in the mass ranges $3 < M_X < 24$ GeV and $M_N < 2$ GeV is:

  $\sigma_D^{partial}/\sigma_{tot} = 6.2 \pm 0.2(stat) \pm 1.4(syst)\%$.

- The effective pomeron intercept derived by fitting the diffractive mass spectrum in the range $8 < M_X < 24$ GeV with the triple pomeron expression is:

  $\alpha_{I\!P}(0) = 1.12 \pm 0.04(stat) \pm 0.08(syst)$.

- If the data in the region $3 < M_X < 24$ GeV are fitted by the sum of two pomeron exchange terms, $I\!P I\!P I\!P$ and $I\!P I\!P I\!R$, assuming $\alpha_{I\!P}(0) = 1.08$ and $\alpha_{I\!R}(0) = 0.45$, the fraction of the $I\!P I\!P I\!R$ term with respect to the sum of the two terms is:

  $f_{I\!P I\!P I\!R} = 26 \pm 3(stat) \pm 12(syst)\%$.

- The fraction of the total photoproduction cross section due to single diffractive photon dissociation, $\gamma p \to Xp$, in the mass range $m_\phi^2 < M_X^2 < 0.05W^2$ is estimated to be:

  $\sigma_{SD}/\sigma_{tot} = 13.3 \pm 0.5(stat) \pm 3.6(syst)\%$.

10 Analysis of the inclusive M_X spectrum

In the analysis described above the identification of the diffractive processes was based on the rapidity-gap signature. The remaining contamination from nondiffractive events satisfying the rapidity-gap requirement was corrected for by using the MC simulation. To test the sensitivity of the results to the model assumptions made in that study we performed another analysis of the same data sample, with a different approach. This time no rapidity-gap was required and the

Table 1. Individual contributions to the systematic uncertainty in the results

source of the uncertainty	$\lvert\Delta\sigma_D^{partial}/\sigma_{tot}\rvert$	$\lvert\Delta\alpha_{I\!P}(0)\rvert$	$\lvert\Delta f_{I\!P I\!P I\!R}\rvert$
nondiffractive contamination	0.9%	0.06	9%
PRT noise and efficiency	0.5%	0.05	7%
diffractive MC model	0.7%	0.03	1%
vector meson production cross section	0.1%	0.01	2%
M_X reconstruction	0.1%	0.01	1%
increased CAL FLT thresholds	0.1%	0.01	1%
M_X fit interval		0.01	2%
value of $b_\circ$		0.01	2%
value of $\alpha_{I\!P}$		0.01	1%

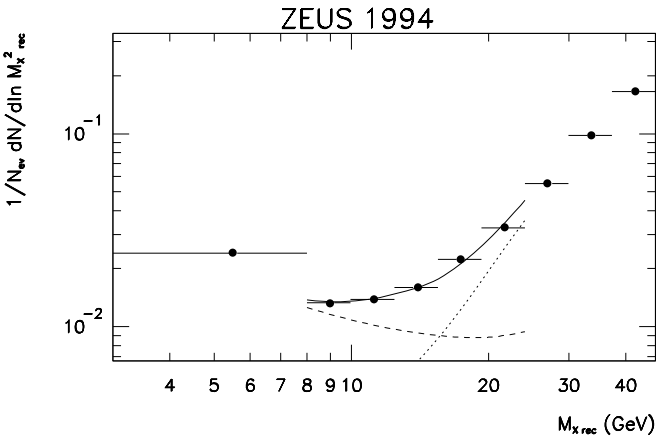

Fig. 9. The uncorrected distribution of reconstructed hadronic mass in photoproduction events at $W \approx 200$ GeV. The *solid curve* shows the result of the fit with the sum of the diffractive and the nondiffractive components, which are also shown separately as *dashed* and *dotted curves*, respectively. The curves correspond to parameterizations (9) and (10) folded with the detector acceptance correction factors which may change the behaviour of the spectrum in the region of the highest and the lowest lnM_X^2 values. The statistical error of the data is smaller than the size of the symbols on the plot

distinction between the different processes was performed solely on the basis of the shape of the mass spectrum [32]. This alternative study is described below.

10.1 Uncorrected spectrum

This analysis was performed on the same sample of photoproduction events used in the previous analysis and selected according to the criteria described in Sect. 5. However, neither the rapidity-gap requirement nor the $\eta_{max} > -1.5$ cut were imposed. This data sample was used to determine the distribution of the reconstructed hadronic mass (see Sect. 7 for details of the mass reconstruction):

$$\frac{1}{N_{ev}} \frac{\Delta N}{\Delta \ln M^2_{X\,rec}}, \tag{7}$$

where N_{ev} is the total number of selected events and ΔN denotes the number of events reconstructed in the given $\ln M^2_{X\,rec}$ bin. The size of the bins $\Delta \ln M^2_{X\,rec}$ was chosen in a similar way to that used in the previous analysis in order to limit the bin-to-bin migrations. The reconstructed mass spectrum obtained in this way is presented in Fig. 9.

10.2 Determination of diffractive and nondiffractive components

The uncorrected mass spectrum was fitted with the sum of the diffractive and nondiffractive components:

$$\frac{1}{N_{ev}} \frac{\Delta N}{\Delta \ln M^2_{X rec}} = A_{ND} \cdot \frac{1}{\sigma_{tot}} \frac{\Delta \sigma_{ND}}{\Delta \ln M^2_X} + A_D \cdot \frac{1}{\sigma_{tot}} \frac{\Delta \sigma_D}{\Delta \ln M^2_X}, \tag{8}$$

where A_{ND} and A_D are M_X dependent correction factors for the nondiffractive and the diffractive components, respectively. They account for the limited acceptance of the trigger and selection cuts as well as for the effects of migrations between the true and the reconstructed mass bins. The true value of M_X^2 for the case of nondiffractive processes was defined as the total invariant mass of hadrons emitted in the angular region covered by the CAL which corresponds to $-3.8 < \eta < 4.3$. The correction factors were obtained from the MC simulation using EPSOFT for the case of nondiffractive processes, and NZ for the diffractive processes.

Similarly to the approach presented in [32], we have assumed that the nondiffractive contribution in the region $M_X^2 < 0.05\ W^2$ may be parameterized by a single exponential form:

$$\frac{1}{\sigma_{tot}} \frac{d\sigma_{ND}}{d \ln M^2_X} = C \exp(B \ln M^2_X). \tag{9}$$

This form can be understood from the assumption of uniform, uncorrelated particle emission in rapidity space. The corresponding M_X distribution is directly related to fluctuations in the number of particles emitted in the angular region covered by CAL. The slope B and the normalization factor C were determined by the fit.

For the diffractive component in (8) a triple pomeron component integrated over t was assumed (see also (6)):

$$\frac{1}{\sigma_{tot}} \frac{d\sigma_D}{d \ln M^2_X} = D \frac{1}{b_\circ + 2\alpha'_{I\!P} \ln \frac{W^2}{M^2_X}} \left(\frac{1}{M^2_X}\right)^{\alpha_{I\!P}(0)-1}. \tag{10}$$

The same values of the parameters $b_\circ$ and $\alpha'_{I\!P}$ as in the rapidity-gap analysis were assumed. The pomeron intercept, $\alpha_{I\!P}(0)$, defining the slope of the diffractive mass distribution and the normalization factor D were determined from the fit.

The result of the fit of expression (8) to the uncorrected mass spectrum in the range $8 < M_{X\,rec} < 24$ GeV is presented in Fig. 9 as a solid curve. The dashed and dotted

curves represent the diffractive and the nondiffractive contributions, respectively.

The slope and the magnitude of the diffractive component is constrained by the low mass behaviour of the measured spectrum. The fit gave a value of $\alpha_{I\!P}(0) = 1.15 \pm 0.08(stat)$. The parameters of the nondiffractive term ((9)) are driven by the rise of the spectrum at large masses where this component dominates. The fit result for the value of the nondiffractive slope is $B = 1.30 \pm 0.08(stat)$.

In the analysis of the rapidity-gap data we observed that in order to describe the diffractive mass spectrum including the low mass region, $3 < M_X < 8$ GeV, a significantly higher value of the effective pomeron intercept is needed. To verify this observation we extended the mass interval used in the present analysis to include also this region. The value obtained for the effective pomeron intercept was $\alpha_{I\!P}(0) = 1.25 \pm 0.08(stat)$, significantly higher than the one obtained previously, though the fit resulted in a poor χ^2. As suggested already in Sect. 9.3 this discrepancy may be due to a contribution of another diffractive term, the $I\!P I\!P I\!R$, in addition to the triple pomeron component. To further test this hypothesis we repeated the fit of the sum of the diffractive and the nondiffractive components to the uncorrected mass spectrum assuming that the diffractive part is a sum of the $I\!P I\!P I\!P$ and the $I\!P I\!P I\!R$ terms. As in the first analysis, the precision of the data was insufficient to determine the individual subprocess contributions as well as the pomeron and reggeon intercepts. Therefore, we assumed the values of $\alpha_{I\!R}(0) = 0.45$ and $\alpha_{I\!P}(0) = 1.08$ and determined the fraction $f_{I\!P I\!P I\!R}$ of the diffractive cross section in the mass interval used for the fit, $3 < M_X < 24$ GeV, due to the $I\!P I\!P I\!R$ term. This was found to be $f_{I\!P I\!P I\!R} = 23 \pm 5(stat)\%$.

Based on the results of the latter fit we derived the fraction of the total photoproduction cross section attributed to the diffractive process, $\gamma p \to XN$, where $3 < M_X < 24$ GeV and $M_N < 5$ GeV, to be $\sigma_D^{partial}/\sigma_{tot} = 5.0 \pm 0.2(stat)$. The limit on the mass of the dissociated proton state is higher than in the case of the rapidity-gap analysis. This is due to the absence of the PRT veto which rejects a large fraction of events with higher M_N, as may be seen from the acceptance plot in Fig. 6. If the diffractive component obtained from the fit is integrated over the mass range $m_\phi^2 < M_X^2 < 0.05W^2$, the cross section for single diffractive photon dissociation relative to the total photoproduction cross section is found to be $\sigma_{SD}/\sigma_{tot} = 11.0 \pm 0.5(stat)\%$.

10.3 Systematic checks

The analysis of systematic uncertainties carried out for these results was similar to that of the rapidity-gap analysis already described in Sect. 9.5. Here, we concentrate only on the two elements that were different.

As (9) and (10) are expected to describe the data up to $M_X^2 < 0.05 \cdot W^2$, we repeated the analysis moving the upper limit on the fitting interval from 24 GeV to 40 GeV. No significant change in the results of the fit was observed.

We also studied the dependence of the results on the M_X binning used. Introducing equal bins in M_X instead of $\ln M_X^2$ we did not observe significant changes in the fit results apart from the value of $\alpha_{I\!P}(0)$ which moved by ± 0.09. This was included into the systematic error.

To estimate the overall systematic uncertainty, all error contributions were added in quadrature.

10.4 Results and comparison with rapidity-gap analysis

The results of this analysis of photoproduction at $W \approx 200$ GeV are:

- The fraction of the total photoproduction cross section attributed to the photon dissociation, $\gamma p \to XN$, in the mass ranges $3 < M_X < 24$ GeV and $M_N < 5$ GeV is:

  $\sigma_D^{partial}/\sigma_{tot} = 5.0 \pm 0.2(stat) \pm 2.0(syst)\%$.

- The effective pomeron intercept derived from the fit of the triple pomeron relation to the diffractive mass spectrum in the range $8 < M_X < 24$ GeV is:

  $\alpha_{I\!P}(0) = 1.15 \pm 0.08(stat) \pm 0.12(syst)$.

- If the data in the region $3 < M_X < 24$ GeV are fitted by the sum of two pomeron exchange terms, $I\!P I\!P I\!P$ and $I\!P I\!P I\!R$, assuming $\alpha_{I\!P}(0) = 1.08$ and $\alpha_{I\!R}(0) = 0.45$, the fraction of the $I\!P I\!P I\!R$ term with respect to the sum of the two terms is:

  $f_{I\!P I\!P I\!R} = 23 \pm 5(stat) \pm 15(syst)\%$.

- The fraction of the total photoproduction cross section due to single diffractive photon dissociation, $\gamma p \to Xp$, in the mass range $m_\phi^2 < M_X^2 < 0.05W^2$ is:

  $\sigma_{SD}/\sigma_{tot} = 11.0 \pm 0.5(stat) \pm 5(syst)\%$.

These numbers should be compared to the results of the first analysis presented in Sect. 9.6. The first of the results, the fraction of the total cross section attributed to photon dissociation, obtained in this analysis should be larger than that obtained in the rapidity-gap study by roughly 5% due to the different M_N limit. However, the precision of the data is too low to establish this difference.

The results of the two analyses are in good agreement. As it was already pointed out, the two analyses differ drastically in the way the diffractive and nondiffractive processes are distinguished:

- In the first analysis the diffractive processes were identified using the rapidity-gap signature and the remaining contamination from nondiffractive processes was corrected for using the MC simulation. This method relies on the MC programs to simulate the effect of the rapidity-gap cut on the nondiffractive processes. However, as the nondiffractive contamination of the final M_X distribution is smaller than in the second method the precision of the results is higher.
- In the second analysis no rapidity-gap was required and the distinction between the different processes was performed solely on the basis of the shape of the mass spectrum. This approach does not require MC simulation of rapidity-gaps in nondiffractive events. However, the larger nondiffractive contamination results in lower precision of the results.

11 Discussion and conclusions

Using the ZEUS detector, we studied the diffractive process $\gamma p \to XN$, where N is either a proton or a nucleonic system with $M_N < 2$ GeV, in photoproduction at high c.m. energy, $W \approx 200$ GeV. Relying on the rapidity-gap signature to identify the diffractive processes we measured the mass spectrum of dissociated photon states in the range $3 < M_X < 24$ GeV. The results were confirmed in an analysis where the distinction between the diffractive and non-diffractive processes was based entirely on the shape of the mass spectrum.

We measured the fraction of the total photoproduction cross section attributed to the diffractive process $\gamma p \to XN$ where $3 < M_X < 24$ GeV and $M_N < 2$ GeV to be:

$\sigma_D^{partial}/\sigma_{tot} = 6.2 \pm 0.2(stat) \pm 1.4(syst)\%$.

By extrapolating beyond the measured M_X interval and correcting for the small contribution of proton dissociation we estimated the cross section for single diffractive photon dissociation, $\gamma p \to Xp$, relative to the total photoproduction cross section to be:

$\sigma_{SD}/\sigma_{tot} = 13.3 \pm 0.5(stat) \pm 3.6(syst)\%$.

This value is consistent with those obtained from other measurements of photoproduction reactions at HERA [4, 5] and with the ones measured in diffractive proton dissociation in $p\bar{p}$ interactions at c.m. energies of $\sqrt{s} = 546$ GeV and 1.8 TeV at the Tevatron [10, 33].

The shape of the diffractive M_X distribution in the region of $8 < M_X < 24$ GeV can be parameterized by the triple pomeron formula with an effective pomeron intercept of:

$\alpha_{I\!P}(0) = 1.12 \pm 0.04(stat) \pm 0.08(syst)$.

This value is in good agreement with those obtained from the shape of the diffractive mass spectrum measured in $p\bar{p}$ interactions at the Tevatron [10].

The cross section for photon dissociation at low masses, $3 < M_X < 8$ GeV, is significantly higher than that expected from the triple pomeron amplitude when using the value of $\alpha_{I\!P}(0)$ derived at higher masses. This behaviour of the M_X spectrum may be due to the contribution of another triple Regge term describing pomeron exchange, namely $I\!P I\!P I\!R$. We verified that the measured spectrum is well described by the sum of the two components with intercepts of $\alpha_{I\!P}(0) = 1.08$ and $\alpha_{I\!R}(0) = 0.45$ [3] derived from fits to total and elastic hadronic cross sections. If these values are assumed, the fit in the interval of $3 < M_X < 24$ GeV indicates that the $I\!P I\!P I\!R$ term is responsible for:

$f_{I\!P I\!P I\!R} = 26 \pm 3(stat) \pm 12(syst)\%$

of the diffractive cross section in the considered M_X range. This size of the $I\!P I\!P I\!R$ contribution is similar to that obtained from the global fits to diffractive dissociation pp data at low energies [11].

To conclude, these studies of the diffractive mass spectrum indicate that the dissociation of real photons at a c.m. energy of $W \approx 200$ GeV is similar to that of hadrons, as expected from the VDM, and it is well described by Regge phenomenology.

Acknowledgements. We thank the DESY Directorate for their strong support and encouragement. The remarkable achievements of the HERA machine group were essential to collect the data used for the present analysis.

References

1. J.J.Sakurai, Ann. Phys. 11 (1960) 1
2. T.H.Bauer et al., Rev. Mod. Phys. 50 (1978) 261
3. A.Donnachie and P.V.Landshoff, Nucl. Phys. B244 (1984) 322; P.V.Landshoff, Nucl. Phys. B(proc.Suppl) 18C (1990) 211
4. H1 Collab., S.Aid et al., Z.Phys. C69 (1995) 27
5. ZEUS Collab., M. Derrick et al., Z. Phys. C63 (1994) 391
6. ZEUS Collab., M. Derrick et al., Z.Phys C69 (1995) 39
7. H1 Collab., S.Aid et al., Nucl.Phys. B463 (1996) 3
8. A.H.Mueller, Phys. Rev. D2 (1970) 2963
9. K.Goulianos, Phys.Rep. 101 (1983) 169; K.Goulianos, Nucl. Phys. B (Proc. Suppl.) 12 (1990) 110
10. CDF Collab., F.Abe et al., Phys. Rev. D 50 (1994) 5535
11. R.D.Field and G.C.Fox, Nucl. Phys. B80 (1974) 367
12. T.J.Chapin et al., Phys. Rev. D31 (1985) 17
13. H1 Collaboration, C.Adloff et al., DESY 97-009, submitted to Z. Phys.
14. D.B.Collins, "An Introduction to Regge Theory and High Energy Physics", Univ. Press (1977)
15. D.B.Collins, A.D.Martin, "Hadron Interactions", Adam Hilger (1984)
16. The ZEUS Detector, Status Report, DESY(1993)
17. ZEUS Collab., M. Derrick et al., Phys. Lett. B293 (1992) 465
18. M. Derrick et al., Nucl. Instr. Meth. A309 (1991) 77; A. Andresen et al., Nucl. Instr. Meth. A309 (1991) 101; A. Bernstein et al., Nucl. Instr. Meth. A336 (1993) 23
19. D. Kisielewska et al., DESY-HERA report 85-25 (1985); J. Andruszkow et al., DESY 92-066 (1992); K. Piotrzkowski, PhD Thesis, Cracow INP-Exp, 1993, DESY F35D-93-06
20. M. Derrick et al., DESY 96-183 (1996), submitted to Z. Phys.
21. B.D.Burow, PhD Thesis, University of Toronto, DESY F35D-94-01 (1994)
22. N.N. Nikolaev and B.G. Zakharov, Z. Phys. C53 (1992) 331
23. P. Bruni et al., Proc. Workshop on Physics at HERA, DESY (1991) 363; A. Solano, PhD Thesis, University of Torino, 1993
24. M.Kasprzak, PhD thesis, Warsaw University, DESY F35D-96-16 (1996)
25. B.R. Webber, Ann. Rev. Nucl. Part. Sci. 36 (1986) 253; G. Marchesini et al., Comput. Phys. Comm. 67 (1992) 465
26. UA4 Collab., D.Bernard et al., Phys. Lett. B166 (1986) 459
27. ZEUS Collab., M.Derrick et al., Z. Phys. C67 (1995) 227
28. UA5 Collab., R.E.Ansorge et al., Z. Phys. C 43 (1989) 357; UA1 Collab., C.Albajar et al., Nucl. Phys. B335 (1990) 261
29. M. Glück, E. Reya and A. Vogt, Phys. Rev. D45 (1992) 3986
30. A. D. Martin, W. J. Stirling and R. G. Roberts, Phys. Lett. B306 (1993) 145
31. T. Sjöstrand, Z. Phys. C42 (1989) 301; H-U. Bengtsson and T. Sjöstrand, Comput. Phys. Commun. 46 (1987) 43; T. Sjöstrand, CERN-TH. 6488/92 (1992)
32. ZEUS Collab., M.Derrick et al., Z. Phys. C70 (1996) 391
33. CDF Collab., F.Abe et al., Phys. Rev. D 50 (1994) 5550